ARTICLE

Cellular and Molecular Biology

MET exon 14 skipping mutation drives cancer progression and recurrence via activation of SMAD2 signalling

Qiaoyan Liang[1,2], Yajun Hu[1,2], Qingyun Yuan[1,2], Min Yu[1,2 ✉], Huijie Wang[3,4 ✉] and Bing Zhao [1,2 ✉]

BACKGROUND: c-Met encoded by the proto-oncogene MET, also known as hepatocyte growth factor (HGF) receptor, plays a crucial role in cellular processes. MET exon 14 skipping alteration (METΔ14EX) is a newly discovered MET mutation. SMAD2 is an important downstream transcription factor in TGF-β pathway. Unfortunately, the mechanisms by which METΔ14EX leads to oncogenic transformation are scarcely understood. The relationship between METΔ14EX and SMAD2 has not been studied yet.
METHODS: We generate METΔ14EX models by CRISPR-Cas9. In vitro transwell, wound-healing, soft-agar assay, in vivo metastasis and subcutaneous recurrence assay were used to study the role of METΔ14EX in tumour progression. RNA-seq, Western blotting, co-immunoprecipitation (CO-IP) and immunofluorescent were performed to explore the interaction between c-Met and SMAD2.
RESULTS: Our results demonstrated that METΔ14EX, independent of HGF, can prolong the constitutive activation of c-Met downstream signalling pathways by impeding c-Met degradation and facilitating tumour metastasis and recurrence. Meanwhile, METΔ14EX strengthens the interaction between c-Met and SMAD2, promoting SMAD2 phosphorylation. Therapeutically, MET inhibitor crizotinib impedes METΔ14EX-mediated tumour metastasis by decreasing SMAD2 phosphorylation.
CONCLUSIONS: These data elucidated the previously unrecognised role of METΔ14EX in cancer progression via activation of SMAD2 independent of TGF-β, which helps to develop more effective therapies for such patients.

BACKGROUND

Oncogene-targeted therapies have significantly improved the survival and prognosis of cancer patients in recent years. The hepatocyte growth factor (HGF) receptor, also known as c-Met, is a receptor tyrosine kinase encoded by the MET oncogene [1]. MET has been demonstrated to be a worthy therapeutic target in various types of tumours due to its multiple roles in cancer development and progression [2, 3], as well as in the acquired resistance to targeted agents, such as epidermal growth factor receptor tyrosine kinase inhibitors (EGFR-TKIs) [4]. However, a number of studies with potentially effective MET inhibitors conducted in unselected cancer patient populations have reported poor curative effects, suggesting the need for a better understanding of the concrete mechanisms underlying different mutations in MET and better selection of patients based on specific MET alterations [5, 6].

In general, the downregulation of c-Met is an essential process preventing receptor oversignaling. Interestingly, all the regulatory mechanisms evidenced so far target the juxtamembrane region of the cytoplasmic part of the receptor, encoded by exon 14 [7]. MET exon 14 contains Y1003, which forms a binding site for CBL, an E3 ubiquitin ligase that targets MET for ubiquitin-mediated degradation [8–10]. Therefore, when exon 14 is skipped, CBL-mediated MET protein degradation is impaired, leading to the accumulation of c-Met and the possibility of oncogenic transformation [11]. In parallel, METΔ14EX is a recurrent event, occurring in approximately 3% of lung adenocarcinomas, 2% of other lung neoplasms, 0.5% of brain gliomas, and 0.5% of carcinomas of unknown primary origin [12, 13].

Recent findings demonstrated that METΔ14EX occurs in mutual exclusivity with mutations in other oncogenes, including EGFR, KRAS, and BRAF mutations, leading to intensified interest in its potential as a therapeutic target [14, 15]. Multivariable analysis revealed that MET exon 14 mutation is an independent poor prognosis factor [16]. In addition, METΔ14EX-mutated patients who undergo targeted therapy tend to have poor long-term survival due to acquired drug resistance [17–19]. As mentioned above, METΔ14EX-driven cancers, where response rates from single-treatment targeted therapies against MET alone remain largely mixed [20, 21]. Unfortunately, how MET exon 14 alteration drives cancer progression and poor prognosis, the specific molecular mechanisms of which are much less explored.

SMAD2 is a member of the SMAD family of proteins that act as downstream effectors in the TGF-β signalling pathway [22, 23].

[1]Key Laboratory of Metabolism and Molecular Medicine, Ministry of Education, Department of Biochemistry and Molecular Biology, School of Basic Medical Sciences, Fudan University, Shanghai, China. [2]Department of Biochemistry and Molecular Biology, School of Basic Medical Sciences, Fudan University, Shanghai, China. [3]Department of Oncology, Shanghai Medical College, Fudan University, Shanghai, China. [4]Department of Medical Oncology, Shanghai Cancer Center, Fudan University, Shanghai, China.
✉email: minyu@shmu.edu.cn; wanghj98@hotmail.com; zhaobing@fudan.edu.cn

Phosphorylation of SMAD2 by TGF-β receptor type I (TβRI) induces a conformational change that allows it to form a complex with SMAD4 and translocate to the nucleus [24]. Once in the nucleus, the SMAD2/SMAD4 complex interacts with other transcription factors to regulate the expression of a variety of target genes. These genes are involved in many cellular processes, including extracellular matrix production, cell cycle regulation, resulting in tumour metastasis and recurrence [25, 26]. Of particular interest, our studies found that c-Met can interact with SMAD2, suggesting that METΔ14EX leads to the phosphorylation and activation of SMAD2. Further research into the mechanisms underlying SMAD2 signalling may provide insight into cancer progression and recurrence in METΔ14EX-altered patients and could lead to the development of new therapeutic strategies.

Therefore, in this study, we sought to dissect the intrinsic role of METΔ14EX in promoting cancer progression and recurrence. We discovered that METΔ14EX resulted in constitutive activation of downstream signalling pathways independent of HGF. We evaluated the effects of METΔ14EX on tumour growth, invasion, metastasis and recurrence. We first revealed the crucial role of METΔ14EX in regulating SMAD2 phosphorylation, which METΔ14EX strengthens the interaction between c-Met and SMAD2, promoting phosphorylation of SMAD2. Finally, we have developed crizotinib, which has demonstrated remarkable tumour inhibition by decreasing SMAD2 phosphorylation in METΔ14EX-altered tumour models. Consequently, a deeper understanding of the molecular background associated with METΔ14EX may suggest novel rational combinatorial or sequential therapeutic strategies to combat drug resistance and improve clinical outcomes.

MATERIALS AND METHODS
CRISPR-Cas9
The gRNAs were designed using the CRISPR Design Tool (http://crispr.mit.edu/) to minimise off-target effects. Four gRNAs separately targeting the splice site of Human-MET exon 14 and Mouse-MET exon 15 were designed and co-transfected into cells to generate METΔ14EX cells. The following gRNAs were used in this study: human-gRNA1: 5′-CACCGTTTCTCTCTGTTTTAAGATC-3′; human-gRNA2: 5′- CACCGTACCGAGCTACTTTTCCAGA-3′; mouse-gRNA1: 5′-CA CCGTAAACTGAATTATACCTTC-3′ and mouse-gRNA2: 5′-CACCGTTAAAGACTTT GCTGTCAC-3′. Oligos were annealed and cloned into the BsmBI site of plasmids lentiCRISPR v2 (Addgene: #52961). The recombinant vector was introduced into 293T cells together with pMD2.G and psPAX2 vectors by PEI method. The virus was collected and infected with tumour cells at 24 and 48 h. The stable mutant cells were screened with puromycin. Finally, single-cell clones were screened by a limited dilution method. Three weeks later, DNA sequencing was performed to isolate METΔ14EX cell clones. The single-cell clone with deletion of exon 14 of two alleles of MET was selected as the METΔ14EX model, while the complete alternating clone of exon 14 was isolated as the wild-type MET model.

Western blotting
Total cellular protein was extracted using RIPA buffer (50 mM Tris-HCl pH 7.5, 150 mM NaCl, 1% NP-40, 0.5% sodium deoxycholate, 0.1% SDS, 1 mM EDTA) supplemented with the protease and phosphatase inhibitor cocktail (Meilunbio, Liaoning, China). Cell lysate was briefly centrifuged for 10 min to remove the insoluble debris. The lysate was separated by SDS-polyacrylamide gel electrophoresis and transferred onto a PVDF membrane. The membranes were soaked in blocking buffer for 1 h, and then incubated with the primary antibody overnight. Anti-phospho-SMAD2 was purchased from GeneTex (Irvine, California). Anti-Akt, anti-phospho-Akt, anti-Erk, anti-phospho-Erk and anti-phospho-Try-1000 were purchased from Cell Signaling Technology (Danvers, MA). Anti-c-Met, anti-SMAD2 were purchased from Proteintech (Chicago, IL). The membranes were exposed to horseradish peroxidase (HRP)-conjugated secondary species-specific antibodies for 1 h (Meilunbio, Liaoning, China).

Co-immunoprecipitation (CO-IP)
Five million A549, Lewis, Hepa1-6 cells were lysed in Lysis buffer (Absin, Shanghai, China) supplemented with the protease and phosphatase inhibitor cocktail (Meilunbio, Liaoning, China) for 30 min on ice and subsequently centrifuged at 14,000 ×g for 10 min. The supernatants were precleared by incubation with ProteinA/G agarose beads (Absin, Shanghai, China) for 60 min at 4 °C. Antibody-coated beads were prepared by incubating rabbit anti-human c-Met antibody (5 μg per sample, Proteintech, Chicago, IL) or control rabbit IgG (5 μg per sample; Proteintech, Chicago, IL) with pre-washed ProteinA/G agarose beads for 2–3 h at room temperature. Lysate was split equally among the c-Met or IgG-coated beads for immunoprecipitation (IP). IP was carried out overnight at 4 °C. Beads were washed, resuspended in loading buffer and proteins were separated on 8% SDS-PAGE followed by transferring to a PVDF membrane and western blotting using indicated antibodies as described by the manufacturer.

Animal studies
This animal study was conducted in accordance with the rules and regulations of the IACUC at the Department of Laboratory Animal Science, Fudan University (Shanghai, P.R. China). C57BL/6 mice (6 weeks old) were raised and treated under specific-pathogen-free conditions.

In vivo metastasis assay
Lewis cells were engineered to express red fluorescent protein to simplify the detection of tumour foci in vivo. A suspension of (1×10^6) tumour cells in 100 μL of phosphate-buffered saline (PBS) was injected into each mouse via tail vein injection ($n = 16$). The physical state of the mice was monitored every day. The mice were randomly divided into two groups: one was killed on the 30th day to observe the metastasis of tumours ($n = 8$), and the other group was used to analyse the survival rate of mice ($n = 8$). On the 30th day after cell injection, 8 mice in each group were randomly selected and euthanised by Chloral hydrate. Lungs and other organs were dissected and the number of metastatic nodules on the lung surface was counted. The remaining mice continued the survival analysis experiment, and the survival results were analysed after 8 weeks.

Subcutaneous recurrence assay
The mice were injected subcutaneously in the right flank with single-cell suspensions of Lewis/Luc cells (1×10^6/100 μL) that expressed detectable luciferase. Both tumour size and body weight were measured three times per week. Tumour volume was measured as indicated time and calculated as follows: $V = (LW^2)/2$, where V is the volume, L is the longest diameter, and W is the shortest diameter. In vivo imaging of mice on the 30th day, animals were administered intraperitoneal D-luciferin (150 mg/kg, Topscience, Shanghai, China), hair near the tumour was shaved off and observed 10 min later by bioluminescence imaging (Opti-Scan Viewn Vivo superior optics, Australia). The bioimaging exposure was 15 s at constant binning. After biological imaging, subcutaneous tumours were surgically removed and the skin was sutured. In vivo imaging was performed on day 1 and day 21 after operation to detect tumour resection and tumour recurrence, respectively.

Xenograft studies and in vivo drug administration
The mice were injected subcutaneously in the right flank with single-cell suspensions of tumour cells (1×10^6/100 μL). Ten days after tumour cell injection, tumour-bearing mice were randomly assigned to receive (1) vehicle; (2) crizotinib (10 mg/kg); via orogastric gavage daily for 30 days. For drug administration, 10 days after tumour inoculation, mice were treated with crizotinib (10 mg/kg). Tumour size and body weight were measured three times per week. The vehicle group was administered 0.5% methylcellulose supplemented with 1% polysorbate-80. Mice were euthanised by Chloral hydrate, and the tumours were removed. Some were fixed in 4% paraformaldehyde and the other tumours were lysed for western blotting.

Statistical analysis
Statistical analyses were conducted using GraphPad Prism 8.0. All data were presented as means ± SD; pairwise multiple comparisons were carried out using two-way ANOVA tests, unpaired t-tests, and log-rank (Mantel–Cox) test. A difference with a value of $p < 0.05$ was considered statistically significant. (***$p < 0.001$; **$p < 0.01$; *$p < 0.05$; ns: not significant $p > 0.05$). All of the experiments were performed at least thrice.
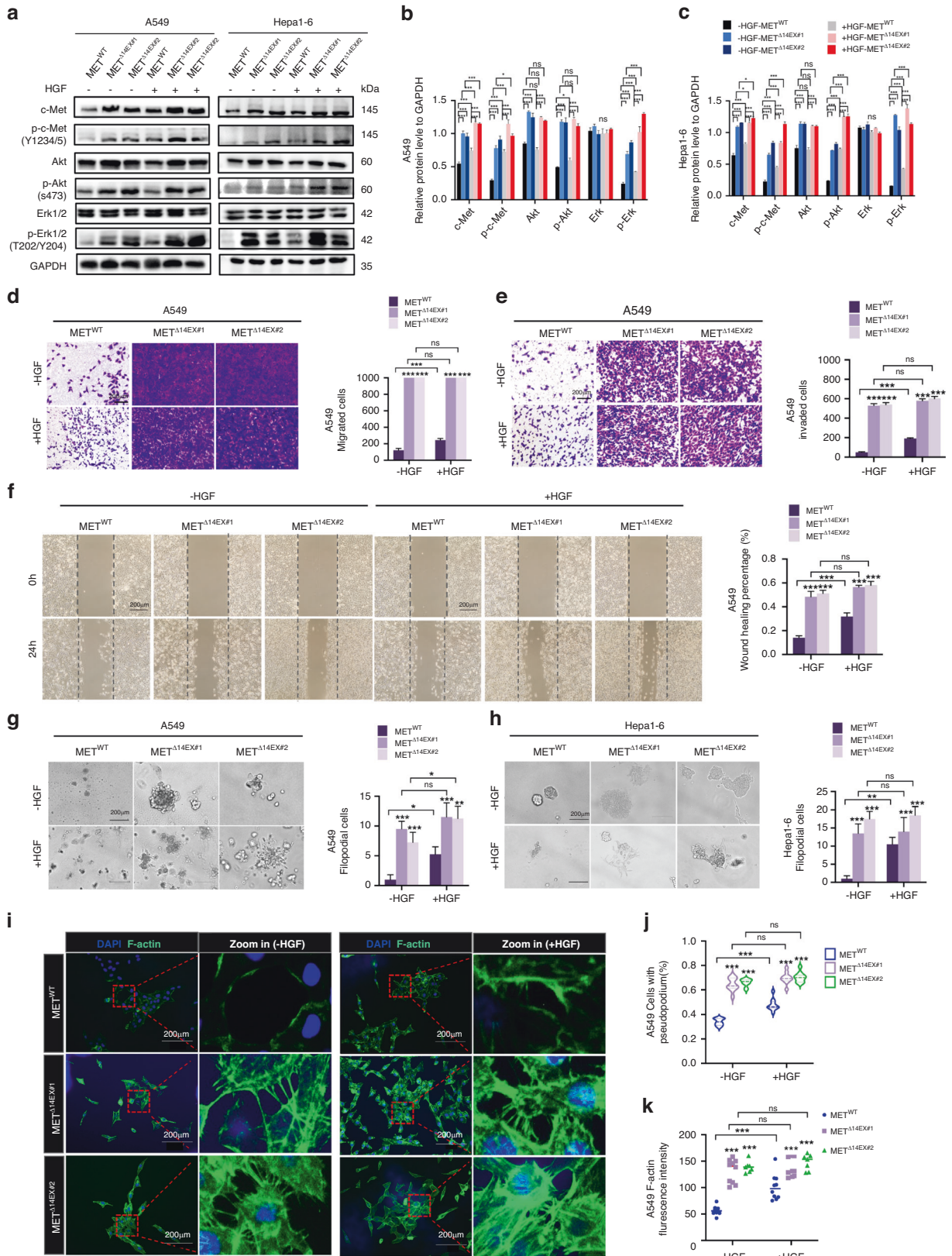
Fig. 1 METΔ14EX alteration promotes cellular migration and invasion in vitro, independent of HGF. a–c Effect of METΔ14EX on downstream signalling. A549 and Hepa1-6 METWT and METΔ14EX cells were treated with PBS, HGF (100 ng/mL) for 30 min, and the phosphorylated and total protein levels of c-Met, Akt, and Erk were measured using western blot. **d** For cell migration detection, transwell inserts in 24-well plates were coated without Matrigel basement membrane matrix. Representative pictures (left) show A549 METWT or METΔ14EX cells (5×10^4/well) that migrated through the transwell. There are too many migrating cells that cannot be counted accurately, they are identified as 1000 migrating cells. Right: quantitative analysis of migrated cells (mean ± SD; $n = 5$). **e** A549 METWT or METΔ14EX cells (5×10^4/well) seeded into Matrigel-coated transwell inserts. Representative pictures (left) of cells invading through the transwell are shown. Right: quantitative analysis of invasive cells (mean ± SD; $n = 5$). **f** A549 METWT and METΔ14EX cells were treated with PBS or HGF (100 ng/mL). The scratch area was photographed, and wound closure was measured. Right: quantitative analysis of the wound area (mean ± SD; $n = 5$). **g, h** Representative images and quantification of A549 (**g**) and Hepa1-6 (**h**) subjected to 3D growth for 14 days (mean ± SD; $n = 5$). **i** Representative images of each group stained with phalloidin in A549 cells. **j** Percentages of ruffle-positive cells in different groups were calculated based on the immunofluorescence. **k** Quantification of the F-actin fluorescence intensity (mean ± SD; $n = 10$). The data shown are means ± SD. ***$p < 0.001$; **$p < 0.01$; *$p < 0.05$; ns not significant $p > 0.05$. Scale bar, 200 μm.

RESULTS

METΔ14EX alteration results in the constitutive activation of downstream signalling pathways independent of HGF

Deletion of MET exon 14, the entire juxtamembrane is caused by several molecular aberrations, such as point mutations, deletions, or indels, that disrupt consensus sequences, including branch sites, polypyrimidine tracts, splice acceptor, and splice donor sites for RNA splicing (Supplementary Fig. S1a).

To investigate the potential tumorigenesis of MET exon 14 skipping alteration in tumour progression, we created several METΔ14EX-mutated cancer cell line models (A549, Lewis, Hepa1-6, and MKN45) using the CRISPR/Cas9 system (Supplementary Fig. S1b) and one single-cell clones formed by single cell was isolated using limiting dilution (Supplementary Fig. S1c). The aberrant METΔ14EX variant was verified at the RNA level using PCR products amplified from cDNA to confirm the deletion of MET exon 14. The METWT was amplified to 529 bp, and the METΔ14EX was amplified to 388 bp (Supplementary Fig. S1d, e). Sequencing confirmed that the monoclonal cell line was a homozygous MET exon 14 knockout cell line (Supplementary Fig. S1f).

Cycloheximide and actinomycin D were added to inhibit the synthesis of protein and RNA, respectively. Western blot experiments showed that c-Met in the METΔ14EX group could not be degraded, but c-Met could be degraded normally in the METWT group. Meanwhile, SMAD2 as a control could be degraded normally in both groups (Supplementary Fig. S2a–f). RT-PCR detection showed that the mRNA of MET degraded normally with time (Supplementary Fig. S2g, h). Therefore, MET exon 14 alteration affects the degradation of c-Met. HGF led to c-Met phosphorylation at Y1234/1235 in both METWT and METΔ14EX cells (Fig. 1a–c and Supplementary Fig. S2i). However, in contrast to a previous study [19], the phosphorylation levels in METΔ14EX cells were both stronger than METWT, whether with or without HGF stimulation. In addition, METΔ14EX delayed c-Met degradation and significantly increased the activity of the PI3K/Akt and MAPK signalling pathways compared with METWT, even without HGF stimulation. Consistently, we found that MET exon 14 skipping alteration leads to the accumulation of c-Met by inhibiting degradation, thus significantly prolonging the constitutive activation of downstream signalling pathways even without HGF-dependent stimulation.

METΔ14EX alteration expedites cellular migration and invasion in vitro independent of HGF

To observe the role of METΔ14EX in tumorigenesis, we conducted transwell-migration assays, transwell-invasion assays, and wound-healing assays to assess the effect of METΔ14EX in cell migration and invasion. The results showed that METΔ14EX significantly increased cell migration, even without HGF stimulation (Fig. 1d and Supplementary Fig. S3a, b). Quantitative analysis of the transwell-invasion assays revealed that METΔ14EX significantly increased cell invasion independent of HGF (Fig. 1e and

Supplementary Fig. S3c, d). Similarly, METΔ14EX obviously enhanced gap closure by approximately 50%, which was higher than the METWT cells, with or without HGF (100 ng/μL) (Fig. 1f and Supplementary Fig. S3e, f). To further validate the role of METΔ14EX in metastasis, METΔ14EX#1 and METΔ14EX#2 cells were placed in 3D Matrigel. After 14 days, cells formed invasive outgrowths (Fig. 1g, h). Due to a substantial body of research, it is well established that filamentous actin (F-actin) plays a pivotal role in the migration of cancer cells. In the context of tumour cell migration, the upregulation of F-actin expression enables cancer cells to overcome tissue barriers, invade blood vessels, and subsequently metastasise to other tissues [27, 28]. As illustrated, METΔ14EX significantly enhanced the fluorescence intensity of polymerised actin (F-actin) compared to METWT cells (Fig. 1i, k and Supplementary Fig. S3g, i). The appearance of membrane ruffles was also increased in METΔ14EX cells (Fig. 1j and Supplementary Fig. S3h). Importantly, HGF enhanced migration and invasion in METWT cells, but not METΔ14EX cells. Together, these results provide strong evidence that METΔ14EX plays a critical role in increasing tumour cell migration and invasion, but is not required for HGF stimulation, which was verified in both lung cancer and liver cancer cells.

METΔ14EX alteration facilitates tumour progression, metastasis and recurrence in vivo

Our results suggest that METΔ14EX plays a critical role in increasing tumour cell migration and invasion in vitro. To further corroborate the role of METΔ14EX alteration in vivo, we conducted xenograft tumour model. In the subcutaneous transplanted tumour model, the tumour volume and weight in the METΔ14EX groups were significantly larger than those in the METWT group (Fig. 2a–d and Supplementary Fig. S4a). The number of mice with lung and liver metastasis was clearly increased in the METΔ14EX groups (Fig. 2e–g).

Similarly, to confirm and extend the effect of METΔ14EX on metastasis in vivo, we injected red fluorescent protein-expressing cells into mice via tail vein (Fig. 2h). It is important to note that the METΔ14EX groups had a shorter survival time compared with METWT (Fig. 2i). We found that METΔ14EX groups had more serious tumour burden and systemic multi-organ metastasis such as lung, liver, heart, kidney and so on (Fig. 2j, k and Supplementary Fig. S4b, c). Moreover, the lungs in the METΔ14EX groups had confluent metastases that were too numerous to count and were clearly enlarged. Histological analysis of lung tissues confirmed that the number of metastatic lesions produced by METΔ14EX cells was significantly increased compared with METWT cells (Fig. 2l, m). We also found that the number of mice with tumour cells colonised in the liver, heart and kidney was largely increased in the METΔ14EX groups compared with the METWT (Supplementary Fig. S4d, e).

As we all know, tumours with the characteristics of malignant proliferation, high invasion, and metastasis generally cause a high
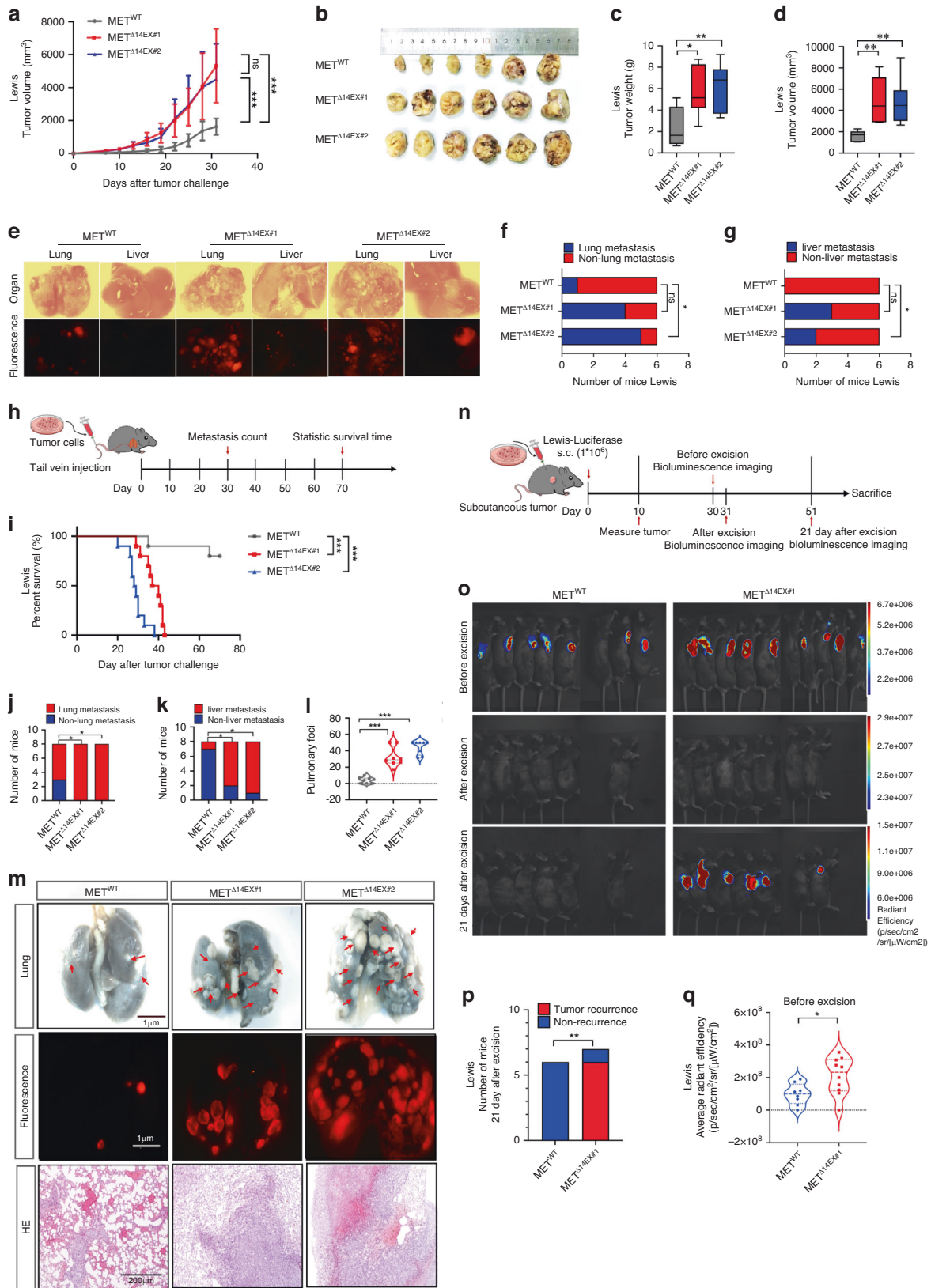
recurrence rate [29]. Therefore, we constructed the subcutaneous tumour recurrence model and found that the probability of tumour recurrence in the METΔ14EX group was much stronger than that in the METWT group, which was verified in both lung cancer and liver cancer models (Fig. 2n–q and Supplementary Fig. S4f–h). Accordingly, our data strongly support that METΔ14EX plays a positive role in promoting tumour growth, metastasis, and recurrence in vivo.

Fig. 2 METΔ14EX alteration enhances tumour progression, metastasis and recurrence in vivo. a–g Mice were injected subcutaneously in the right flank with single-cell suspensions of tumour cells (1×10^6). **a** Serial measures of tumour volume were taken after cells were transplanted into mice. **b** Mice were humanely killed, and the tumours were resected 31 days after cell injection. **c** The weight of the resected tumours was determined. **d** The volume of the resected tumours was determined. **e** Representative photograph of lung and liver-bearing tumours are shown (upper); the gross appearance of representative lung and liver harvested is viewed under a fluorescence stereoscope (bottom). **f** The number of mice with tumour cells in the lung is recorded. **g** The number of mice with tumour cells in the liver is recorded. **h–m** Lewis METWT and METΔ14EX cells were delivered by tail vein injection into mice. Lewis cells were engineered to express red fluorescent protein to simplify detection of tumour foci in vivo. **h** Flowchart of in vivo metastasis assay. **i** The survival of mice in different groups is shown. **j** The number of mice with lung metastasis is recorded. **k** The number of mice with liver metastasis is recorded. **l** The number of metastatic nodes per lung was determined in different groups. **m** The effect of METWT and METΔ14EX cells on the formation of metastatic nodes on the 30th day is shown. **n–q** Mice were injected subcutaneously in the right flank with single-cell suspensions of Lewis/Luc cells (1×10^6) that expressed detectable luciferase. In vivo imaging of mice on the 30th day, animals were administered intraperitoneal D-luciferin by bioluminescence imaging. Then the subcutaneous tumour was surgically removed and the skin was sutured. In vivo imaging was performed on day 1 and day 21 after operation to detect tumour resection and tumour recurrence. **n** Flowchart of in vivo subcutaneous tumour recurrence model. **o** In vivo imaging of each group is conducted on the 30th, 31st, and 51st days after cell injection. **p** The number of mice with tumour recurrence is recorded. **q** The average radiant efficiency of each group before excision is shown. The data shown are means ± SD. ***$p < 0.001$; **$p < 0.01$; *$p < 0.05$; ns: not significant $p > 0.05$. Scale bar, 1 μm.

METΔ14EX alteration upregulates dominant cell movement-associated gene signatures

To investigate the potential mechanism underlying METΔ14EX alteration in tumour metastasis, we performed RNA-seq in METWT and METΔ14EX cell lines without HGF and in tumour tissue in the mouse xenograft model. We identified 782 differentially expressed genes (DEGs) between METWT and METΔ14EX cell lines using the criteria of adjusted p value (<0.05) and fold change (logFC > 1 or < 1) (Fig. 3a, b). The difference in DEG numbers without HGF treatment suggests the potential dynamic effects of HGF-independent stimulation between METWT and METΔ14EX cell lines. In the absence of HGF, the Gene Ontology (GO) analysis revealed that cell movement-associated biological processes were positively enriched, and multiple gene sets, including cell junction, adherens junction, anchoring junction, focal adhesion, filopodium, and extracellular space, were top-ranked (Fig. 3c). The same conclusion is obtained from the analysis of RNA-seq in METWT and METΔ14EX tumour tissue in the mouse xenograft model. The Ingenuity Pathway Analysis (IPA) 'Regulator Effects' algorithm connects upstream regulators, dataset molecules, and downstream functions or diseases [30]. The top-ranked 'Regulator Effects' based on METWT and METΔ14EX tumour tissue in Kyoto Encyclopedia of Genes and Genomes (KEGG) also suggested that most identified downstream biological functions were associated with cell invasion and metastasis, such as regulation of actin cytoskeleton, collagen degradation, Extracellular Matrix (ECM) proteoglycans, non-integrin membrane-ECM interactions, collagen chain trimerisation, collagen biosynthesis and modifying enzymes, integrin cell surface interactions and Rho GTP cycle (Supplementary Fig. S5a). Together, these results strongly support that hyperactivation of METΔ14EX-mediated signalling elicits a strong and concerted activation of the cell movement machinery.

METΔ14EX alteration significantly prolongs the activation of SMAD2 signalling via promoting phosphorylation of SMAD2

The KEGG pathway analysis indicated that TGF-β signalling pathway was top-ranked (Fig. 3d), suggesting its downstream targeted gene sets were upregulated. TGF-β signalling pathway is a well-known potent driver of cancer progression through Epithelial-Mesenchymal Transition (EMT) [31]. As the most critical downstream transcription factor in activating the TGF-β signalling pathway, SMAD2 can bind to the promoters of genes downstream of TGF-β signalling pathway when it is activated into the nucleus [32]. Immunoblotting showed elevated levels of phospho-SMAD2 in the METΔ14EX group compared with METWT, with or without HGF. And HGF did not affect the SMAD2 phosphorylation level of the METΔ14EX groups, but slightly increased the phosphorylation level of the METWT group (Fig. 3e, f and Supplementary Fig. S5b–e). Meanwhile, immunofluorescence showed that more

SMAD2 in METΔ14EX groups entered the nucleus, compared with METWT (Fig. 3g). The pathway analysis conducted previously has confirmed that METΔ14EX significantly prolong the activation of SMAD2 signalling.

However, it is still unclear whether METΔ14EX regulates the activation of SMAD2. To further confirm the relationship between c-Met and SMAD2, cells were treated with the c-Met inhibitor JNJ38877605 with a concentration gradient for 24 h. We observed that the SMAD2 phosphorylation began to be inhibited at 100 nM, and the inhibitory effect was the most significant at 300 nM (Fig. 4a and Supplementary Fig. S6a). At the concentration of 300 nM, the inhibitory effect of JNJ38877605 on SMAD2 phosphorylation increased with the extension of treatment time (Fig. 4b, c). In the TGF-β signalling pathway, SMAD2 is phosphorylated by TGF-β receptor type I (Tβ RI), which activates the signalling pathway [24]. To further verify that SMAD2 could phosphorylated by c-Met, we added the TGF-β receptor type I/II (Tβ RI/II) dual inhibitor LY2109761 and c-Met inhibitor JNJ38877605 separately. Immunoblotting showed that the addition of both inhibitors partially inhibited SMAD2 phosphorylation, while the combination had a stronger inhibitory effect (Fig. 4d, e and Supplementary Fig. S6b, c). In addition, it was observed that the METWT group did not exhibit the same impact. This could be attributed to the inactive c-Met in METWT group, resulting in inadequate levels of SMAD2 phosphorylation (Fig. 4e). In order to further prove that activated c-Met can phosphorylate SMAD2 independent of TGF-β ligand, we detected the change of SMAD2 phosphorylation by adding Tβ RI/II dual inhibitor for 12 h and then adding HGF to stimulate for 15 min. The results showed that 15 min transient stimulation could directly upregulate the level of SMAD2 phosphorylation and did not affect the expression of TGF-β (Fig. 4f). This suggests that the promotive activation of c-Met in the METΔ14EX group may enhance SMAD2 phosphorylation independent of TGF-β.

To explore whether there is an interaction between c-Met and SMAD2, we used the ZDOCK database by Discovery Studio, a computer protein simulation software, to predict the binding mode of SMAD2 (PDB ID: 1KHX) with c-Met (PDB ID: 4GG7). The simulation showed that there are some interaction interfaces between the phosphorylated region of SMAD2 (white arrow in Fig. 4g) and the kinase active region of c-Met (yellow region in Fig. 4g). To further validate c-Met has an interaction with SMAD2, we performed CO-IP assay and found that c-Met can bind to SMAD2 with or without HGF, in both the METΔ14EX and METWT groups (Fig. 4h and Supplementary Fig. 6d, e). Nevertheless, compared with the METWT group, the METΔ14EX groups exhibited a higher capacity to bind SMAD2 and elevated SMAD2 phosphorylation levels. This suggests that the METΔ14EX-activated-c-Met is capable of efficiently binding to and
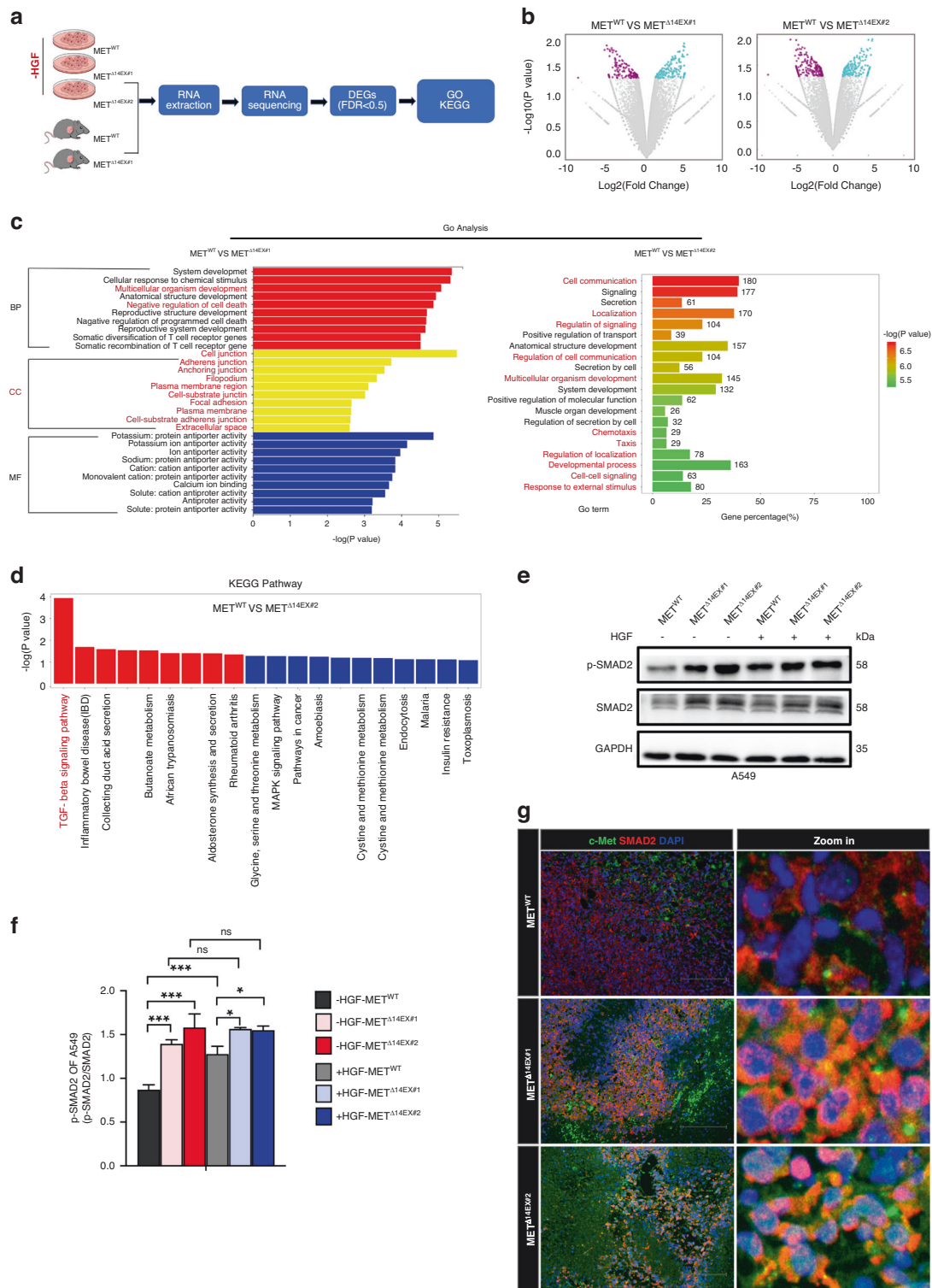
Fig. 3 RNA-seq analysis reveals that METΔ14EX alteration remarkably upregulated dominant cell movement-associated gene signatures. **a** Schematic diagram of the experimental design and analysis workflow for RNA sequencing. **b** The volcano plots display the distribution of differentially expressed genes (DEGs) identified in A549 METΔ14EX versus METWT cells. The x-axis represents the log2-fold change of each gene, and the y-axis represents the log10 transformation of p values. Genes with a fold change >2 and p value of <0.05 were considered significant DEGs. Upregulated genes are indicated in blue, downregulated genes in purple, and nonsignificantly altered genes in grey. **c** GO analysis was used to analyse the DEGs in A549 METΔ14EX groups versus METWT. The top enriched biological processes based on GO are ranked according to the normalised enrichment scores (NES). **d** The KEGG analysis was conducted on the expression profile of a group of DEGs (METΔ14EX vs. METWT). **e** A549 METWT and METΔ14EX cells were treated with PBS, HGF (100 ng/mL) for 30 min, and the phosphorylated and total protein levels of SMAD2 were measured using western blot. GAPDH was used as the loading control. **f** The summary data of western blotting show the level of p-SMAD2 in A549. **g** The representative images of SMAD2 into the nucleus in METWT and METΔ14EX groups based on the immunofluorescence. The data shown are means ± SD. ***$p < 0.001$; **$p < 0.01$; *$p < 0.05$; ns not significant $p > 0.05$.
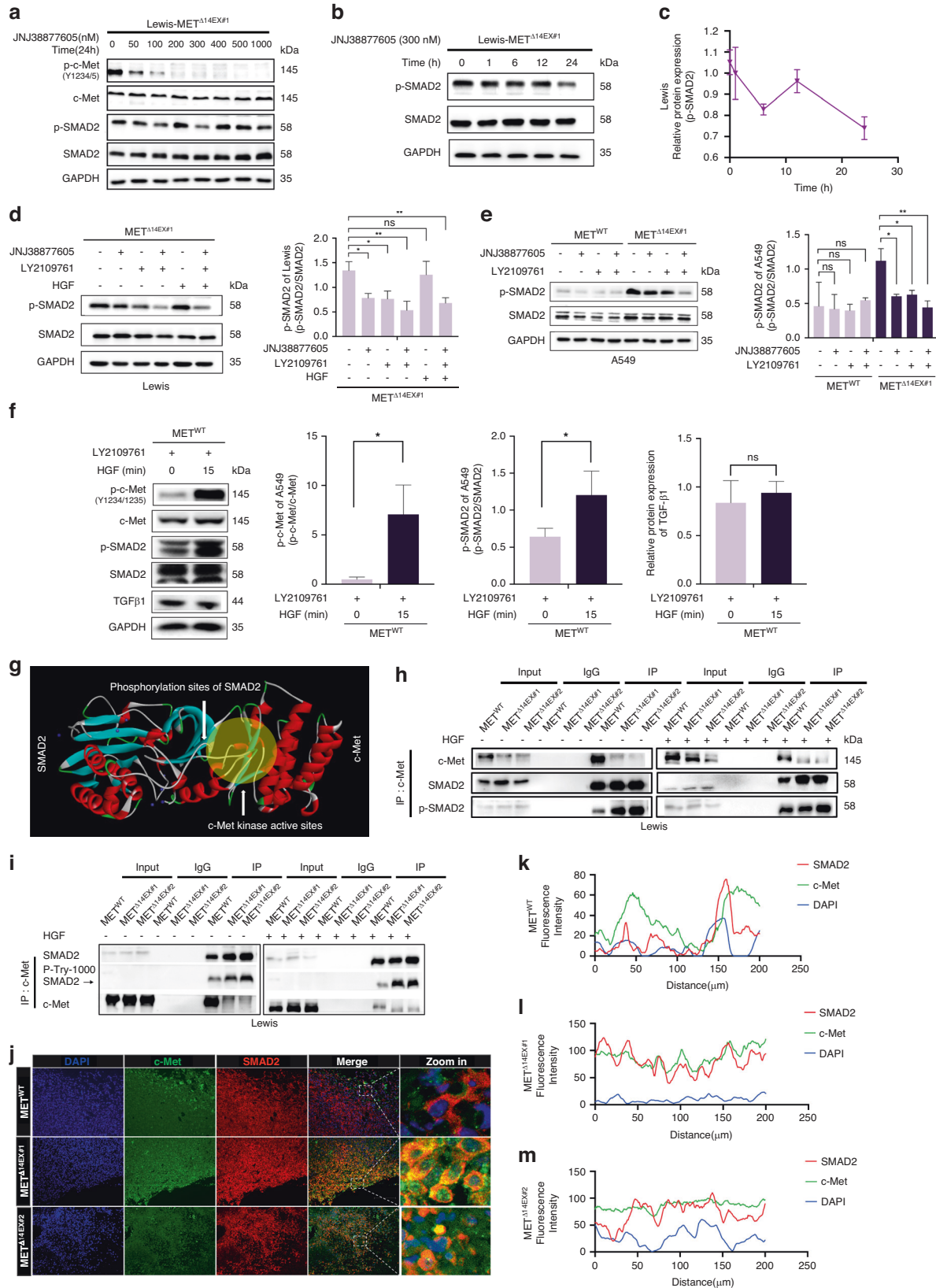
phosphorylating SMAD2. Notably, c-Met is a receptor tyrosine kinase [33]. Our investigation delved deeper into how MET Δ14EX regulates SMAD2 phosphorylation. The findings suggest that SMAD2 can be phosphorylated at tyrosine residues in a MET kinase-dependent manner. Interestingly, we observed that the tyrosine kinase activity of SMAD2 in the METWT group was significantly lower than that in METΔ14EX groups (Fig. 4i and Supplementary Fig. S6f, g). To further validate their interaction

Fig. 4   METΔ14EX alteration activates SMAD2 signalling via promoting phosphorylation of SMAD2. a Western blotting analysis showed the concentration gradient of the phosphorylated and total protein levels of c-Met and SMAD2 in Lewis cells treated with c-Met inhibitor JNJ38877605 (24 h). GAPDH was used as the loading control. **b** Western blotting analysis was performed to detect the phosphorylation of SMAD2 at different time points in Lewis cells treated with JNJ38877605 (300 nM). **c** The summary data of western blotting show the level of p-SMAD2 in Lewis. **d** Western blotting analysis showed the phosphorylation of SMAD2 in Lewis cells treated with JNJ38877605 and LY2109761 (300 nM for 24 h). Right, summary data of western blotting show the level of p-SMAD2 in Lewis ($n = 3$). **e** Western blotting analysis showed the phosphorylation of SMAD2 in A549 cells. Right, summary data of western blotting show the level of p-SMAD2 in A549. **f** Western blotting analysis showed the phosphorylation of c-Met, SMAD2 and relative protein expression of TGF-β1 in A549 cells. Right, summary data of western blotting. **g** The ZDOCK database from Discovery Studio was used to predict the binding mode of SMAD2 (PDB ID: 1KHX) with c-Met (PDB ID: 4GG7). **h** CO-IP analysis revealed that c-Met interacts with SMAD2 and p-SMAD2 in Lewis cells. **i** Western blotting analysis was performed to detect SMAD2 tyrosine phosphorylation after immunoprecipitation from Lewis cells. **j** Representative pictures of immunostaining of c-Met and SMAD2 was performed in Lewis METWT and METΔ14EX tumour sections. **k**–**m** The quantitative analysis of colocation of c-Met and SMAD2 in METWT and METΔ14EX groups. The data shown are means ± SD. ***$p < 0.001$; **$p < 0.01$; *$p < 0.05$; ns: not significant $p > 0.05$. Scale bar, 200 μm.

relationship, we generated mutants of key amino acids within critical structural domains of the c-Met. We utilised CO-IP assay to reconfirm changes in interaction. The results revealed that when the crucial amino acids Y1349 and Y1356 in the binding region of c-Met were mutated, the binding with SMAD2 significantly decreased. However, when the key amino acids Y1234 and Y1235 in the tyrosine kinase domain of c-Met were mutated, it did not alter the interaction with SMAD2 but reduced the phosphorylation of SMAD2. Notably, mutations in the Y1230 amino acid did not result in corresponding changes (Supplementary Fig. S6h–j). These findings suggest that the activated c-Met, acting as a receptor tyrosine kinase, interacts with SMAD2, leading to the robust phosphorylation of SMAD2 and promoting downstream signalling. Then, we analysed the colocation of c-Met and SMAD2 by immunofluorescent detection, providing evidence that obvious protein colocalisation was found in METΔ14EX groups compared with METWT (Fig. 4j–m). These findings clearly demonstrate the key role of METΔ14EX alteration in the promotion of tumour progression and recurrence via significantly prolonging the activation of SMAD2 signalling.

Knocking down SMAD2 dramatically represses METΔ14EX-mediated tumour metastasis

To further confirm that METΔ14EX alteration promotes tumour metastasis through SMAD2 signalling pathway, we generated SMAD2 knockdown cell lines (Fig. 5a, b). Wound-healing and transwell-migration assays revealed that knocking down SMAD2 significantly inhibited cell migration in the METΔ14EX group. In the METWT group without HGF, SMAD2 knockdown had no significant effect on migration. However, after c-Met activation, knocking down SMAD2 also inhibited cell migration (Fig. 5c, d). Consistent with these findings, transwell-invasion assays yielded the same results (Fig. 5e).

To further validate these results in vivo, we used a metastasis model and found that knocking down SMAD2 could prolong survival time and reduce multi-organ metastasis of the tumour in the METΔ14EX group, particularly in the lungs and liver. However, there was no difference in the METWT group (Fig. 5f–k). Taken together, these results provide further evidence that METΔ14EX-mediated tumours promote metastasis by enhancing the activated c-Met/SMAD2 signalling.

MET inhibitor crizotinib effectively represses METΔ14EX-mediated tumour progression by decreasing SMAD2 phosphorylation

Thus far, our studies revealed that METΔ14EX alteration significantly increases tumour invasion, metastasis and recurrence primarily by upregulation of the SMAD2 signalling pathway and numerous genes involved in activation of cell movement-associated biological processes, as well as enhancement of tumour-associated angiogenesis. Based on the pivotal role of METΔ14EX in tumour progression, we investigated the

effect of the selected potent MET inhibitor crizotinib on METΔ14EX-mediated tumour progression. We found that crizotinib could completely eliminate cell migration, invasion, and wound healing in METΔ14EX cells (Fig. 6a, b). On the basis of these results, we tested the role of MET inhibitors on the xenograft tumour model, crizotinib showed potent inhibitory effects on tumour growth, and it has no effect on the weight of mice (Fig. 6c–j). We found crizotinib administration significantly repressed tumour cell progression. Furthermore, observed METΔ14EX-enhanced signalling output, including phospho-Erk, was repressed to relatively low levels (Fig. 6k). Most importantly, crizotinib could greatly inhibit the phosphorylation of SMAD2, suggesting that crizotinib had a mighty inhibitory function on phosphorylation and activation of SMAD2 (Fig. 6k). These results indicate that crizotinib is an effective clinical drug choice for patients with METΔ14EX alteration, as it effectively represses METΔ14EX-mediated tumour progression via inhibiting the activation of SMAD2.

DISCUSSION

METΔ14EX is usually mutually exclusive with other recognised carcinogenic drivers and is reported to be present in a range of malignant tumours, which is identified as key oncogenic drivers and a viable therapeutic target, similar to other oncogenic drivers, highlighting the critical role of METΔ14EX itself as a driver mutation [34, 35]. More importantly, the underlying mechanisms by which METΔ14EX promotes tumour progression remain poorly understood. Therefore, the assessment of METΔ14EX alteration has become an important step in clinical management, particularly for advanced cancer patients [36, 37]. Moreover, recent research works on the response to targeted therapy in patients with METΔ14EX alteration provide further evidence of potential clinical benefits [38]. Furthermore, MET exon 14 skipping alteration has been implicated in resistance to targeted therapies and immunotherapy in various cancers [39, 40], making it a crucial biomarker for predicting treatment response. Therefore, further research dissecting the molecular signalling steps involved in METΔ14EX-driven tumorigenesis as well as unique mesenchymal differentiation will offer opportunities to highlight potential molecular targets that can be targeted for alternative and combination approaches for more effective therapies. Our investigative findings have resulted in significant revelations regarding the mechanisms by which METΔ14EX stimulates the receptor kinase's activity, ultimately facilitating cell migration, invasion, metastasis and recurrence.

In this study, we investigated the tumorigenic role of METΔ14EX in tumour invasion, metastasis, and recurrence. Initially, we successfully constructed several homologous cell models in various tumours using the CRISPR genome editing system to simulate the METΔ14EX alteration produced by the natural non-overexpression scenarios. Our findings indicate that the c-Met in

a

b

c

d

e

f

g

h

i

j

k
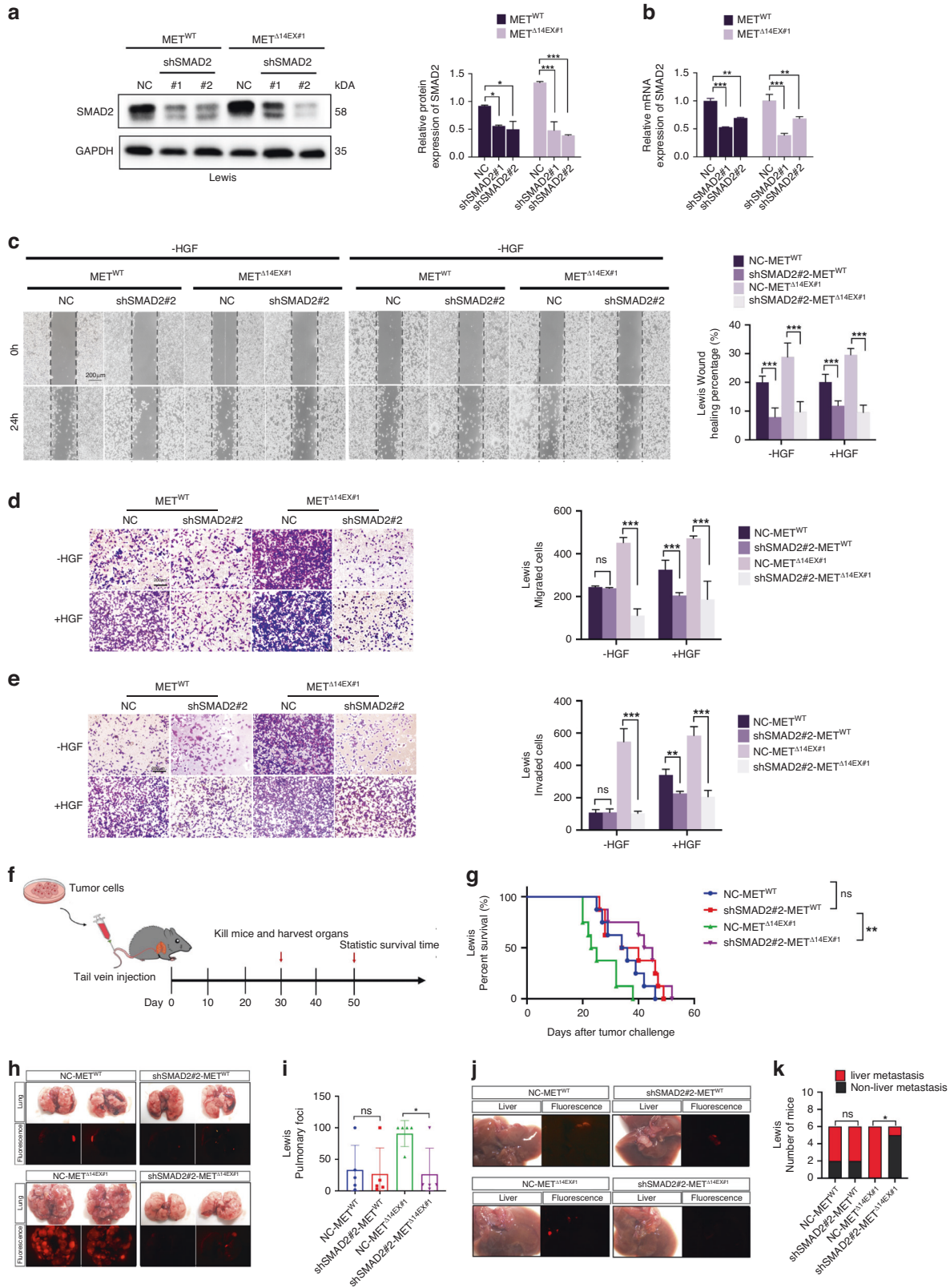
tumour cells with METΔ14EX alteration does not degrade over time, although the RNA degradation remains unaffected. Studies have suggested that E3 ligase C-CBL is the primary regulator of MET endocytosis through interaction with MET juxtamembrane

(JM) region [10]. Therefore, the absence of the juxtamembrane region in METΔ14EX weakens its interaction with C-CBL, resulting in the escape of METΔ14EX endocytosis [30]. As a result, METΔ14EX has enhanced and persistent activity due to

Fig. 5 METΔ14EX-mediated tumour metastasis through activation of SMAD2 signalling. a Western blotting shows knockdown of SMAD2 in Lewis METWT and METΔ14EX cells compared with negative control. The right panel shows summary data of western blotting. **b** RT-PCR shows knockdown of SMAD2 in Lewis METWT and METΔ14EX cells compared with negative control. **c** Lewis cells were treated with PBS or HGF (100 ng/mL), and the scratch area was photographed, and wound closure was measured. The right panel shows quantitative analysis of wound area (mean ± SD; $n = 5$). **d** Representative pictures (left) show Lewis cells (5×10^4/well) migrated through the transwell. For cell migration detection, transwell inserts in 24-well plates were coated without Matrigel basement membrane matrix. The right panel shows quantitative analysis of migrated cells (mean ± SD; $n = 5$). **e** Representative pictures (left) show Lewis cells (5×10^4/well) invaded through the transwell. Lewis cells seeded into Matrigel-coated transwell inserts. The right panel shows quantitative analysis of invasive cells (mean ± SD; $n = 5$). **f–k** In vivo metastasis assay. **f** 1×10^6 Lewis NC-METWT, shSMAD2#2-METWT, NC-METΔ14EX, shSMAD2#2-METΔ14EX cells were delivered by tail vein injection into mice. **g** The survival of mice in different groups is shown. **h** Representative photographs of lung show the effect of the formation of metastatic nodes on the 30th day. **i** Quantitative analysis shows the number of metastatic nodes per lung determined in different groups. **j** Representative photographs of liver show the effect of the formation of metastatic nodes on the 30 day. **k** The number of mice with liver metastasis is recorded. The data shown are means ± SD. ***$p < 0.001$; **$p < 0.01$; *$p < 0.05$; ns not significant $p > 0.05$. Scale bar, 200 μm.

degradation impairment, which in turn promotes cell migration and invasion in vitro independent of HGF, as well as metastasis and recurrence in vivo. Overexpression of MET has previously been linked to metastasis and poor prognosis [41, 42]. Some findings suggest that the overactivation of the HGF/MET signalling is the primary source of cell movement and metastasis [13, 43]. However, our experiments demonstrate that the phenotype of invasion and metastasis induced by METΔ14EX does not require stimulation by HGF, highlighting the independence and importance of METΔ14EX itself as a key regulator. Through its own constitutive activation, it promotes the malignant process by providing tumour cells with metastatic potential.

Considering the phenotype of invasion and metastasis triggered by METΔ14EX as 'extrinsic evidence', further 'intrinsic evidence' can be obtained through an analysis of the molecular mechanisms involved. The examination of HGF-independent changes in the transcriptional signature under METΔ14EX strongly supports its independent role as a critical promoter of cell invasion and metastasis. The enriched functional and signalling pathways identified in both GO and KEGG are closely associated with cell movement, which is facilitated by the activation of METΔ14EX signalling. This activation results in the upregulation of genes related to cell cytoskeleton and cell-matrix adhesion reorganisation such as collagen degradation, ECM proteoglycans, non-integrin membrane-ECM interactions, collagen chain trimerisation, collagen biosynthesis and modifying enzymes, integrin cell surface interactions and Rho GTP cycle and so on, both of which are crucial processes in driving cell movement. As such, these findings suggest that following tumorigenesis, METΔ14EX may primarily regulate cell migration and invasion, rather than cell growth.

Intriguingly, the KEGG pathway analysis indicated that TGF-β signalling pathway was top-ranked in METΔ14EX without HGF (vs. METWT) (Fig. 3d and Supplementary Fig. S5b), suggesting its downstream targeted gene sets were upregulated. TGF-β plays a dual role in tumorigenesis by inhibiting tumour growth in the early stages and promoting tumour growth. Importantly, TGF-β can also induce the formation of a microenvironment conducive to tumour metastasis [44] and promote tumour epithelial-mesenchymal transition (EMT) by inducing the expression of transcription factors such as Snail1/2, ZEB1/2, and HMGA2 [45–47]. SMAD2 is the critical downstream transcription factor in the TGF-β pathway [32], which is phosphorylated by TβRI receptor to activate the pathway. The canonical function of SMAD2 in mediating TGF-β signalling is well established. However, several studies show that SMAD2 signalling can be activated by stimuli other than the ligands in the TGF-β superfamily [48]. According to our findings, using the ZDOCK database of Discovery Studio, the simulation showed that there are interaction interfaces between the phosphorylated region of SMAD2 (white arrow in Fig. 4f) and the kinase active region of c-Met (yellow region in Fig. 4f). Likewise, CO-IP assay and immunofluorescent analysis validated that METΔ14EX

strengthens the interaction between c-Met and SMAD2. Then, to further verify that c-Met can phosphorylates SMAD2, we added the Tβ RI/II dual inhibitor LY2109761 and c-Met inhibitor JNJ38877605 separately. Immunoblotting showed that the addition of both inhibitors partially inhibited SMAD2 phosphorylation, while the combination had a stronger inhibitory effect (Fig. 4d, e and Supplementary Fig. S6b, c). In addition, knockdown of SMAD2 can dramatically repressed METΔ14EX-mediated tumour metastasis. In contrast to the METΔ14EX group, knockdown of SMAD2 in the METWT group did not hinder the invasion and migration of tumour cells in vitro or tumour metastasis in vivo. In other words, it appears that the SMAD2 signal pathway is not activated in the METWT group, and therefore does not contribute to the promotion of cancer. Conversely, in the METΔ14EX group, the SMAD2 signal pathway is activated, thereby initiating the signal transduction that leads to cancer promotion. Hence, our data implicated that METΔ14EX-mutated protein can bind and robustly phosphorylate SMAD2, promoting excessive activation of the SMAD2 signalling pathway independent of TGF-β ligand, thereby promoting tumour metastasis and recurrence. This may be due to the massive accumulation of the METΔ14EX-altered c-Met after constitutive activation, leading to dimer tyrosine phosphorylation, and subsequently binding to and phosphorylating SMAD2.

Notably, effective MET-TKIs (Mesenchymal to Epithelial Transition factor – Tyrosine Kinase Inhibitors) have shown high response rates and lasting benefits, making them a potential first-line treatment option for patients with lung adenocarcinoma [49–51]. Our results now provide compelling preclinical evidence to better define the effect of MET inhibitors. Namely, crizotinib not only remarkably inhibited the constitutive activation of downstream signalling, but also inhibited SMAD2 signalling and repressed cell migration and invasion in vitro and tumour progression in vivo. Thus, the blockade of METΔ14EX/SMAD2 signalling using MET inhibitors is a potent therapeutic option for METΔ14EX-mutated patients.

In conclusion, all the above findings and considering the key role of the above factors in METΔ14EX -mediated tumour progression can be similarly verified in hepatocellular carcinoma cell lines, which suggests that METΔ14EX alteration promoting tumour invasion and metastasis may have the same mechanism in several kinds of tumours. In conclusion, our study highlights the oncogenic role of METΔ14EX alteration in various tumours and sheds light on the underlying mechanism through which METΔ14EX drives tumour invasiveness and metastasis by upregulating global gene transcripts and key signal pathways. More notably, our findings strikingly demonstrate that METΔ14EX positively affects key factors in cancer progression and recurrence via a non-canonical activation of SMAD2 signalling independent of TGF-β ligand. Given the critical role of these factors in tumour progression, our study provides a basis for exploring new inhibition strategies for more effective and lasting treatment of patients with METΔ14EX mutation.
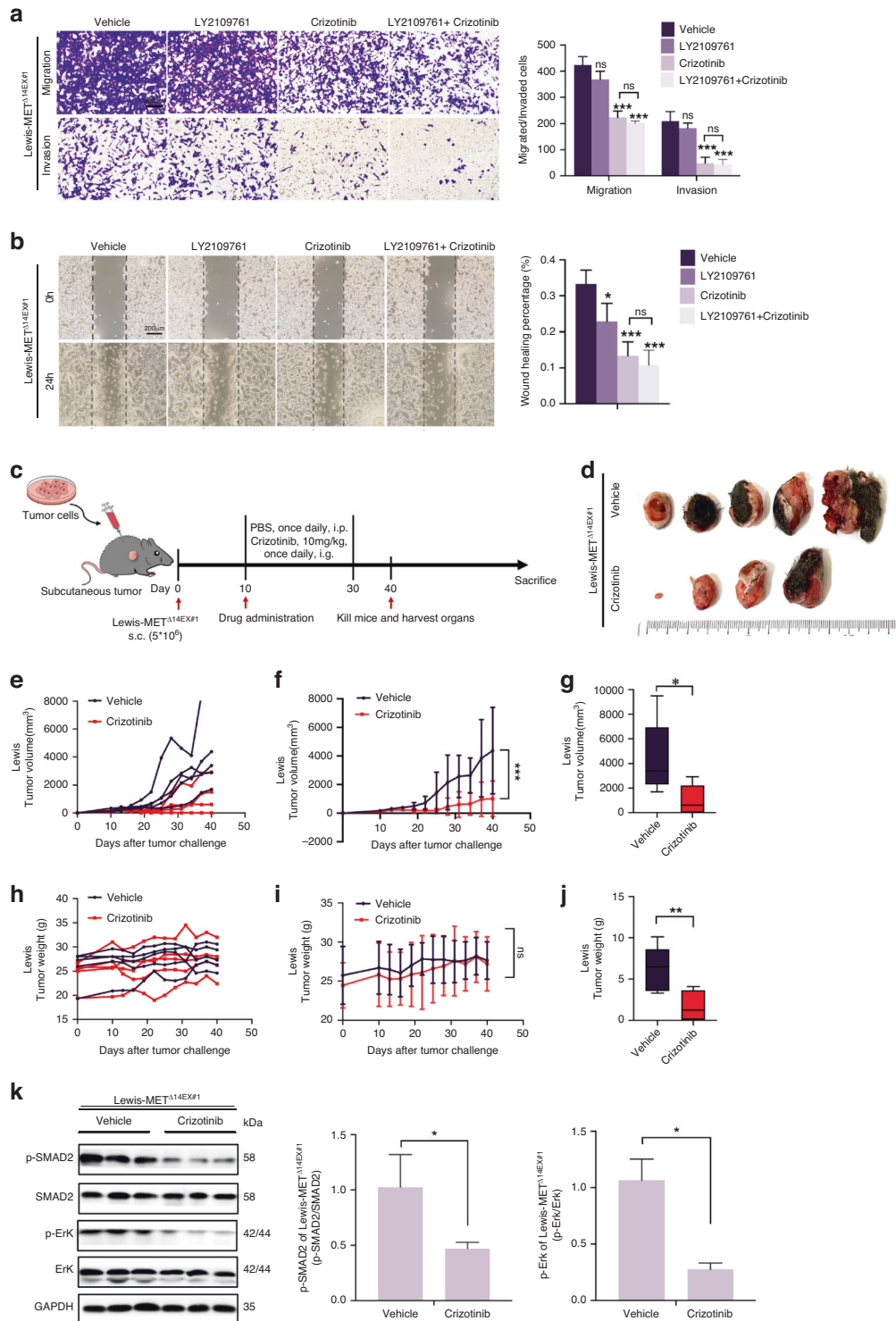
Fig. 6 Crizotinib dramatically represses METΔ14EX-mediated tumour growth as well as metastasis. a Representative pictures (left) of migrated (upper) and invasive (bottom) Lewis cells (5×10^4/well) through transwell inserts are shown. Right: quantitative analysis of migrated and invasive cells (mean ± SD; $n = 5$). **b** The scratch area was photographed and wound closure was measured for different groups. Right: quantitative analysis of the wound area (mean ± SD; $n = 5$). **c–j** Mice were injected subcutaneously in the right flank with single-cell suspensions of tumour cells (1×10^6). For drug administration, 10 days after tumour inoculation, mice were either treated with PBS (Vehicle) or Crizotinib (10 mg/kg). **c** Flowchart of in vivo metastasis assay. **d** Mice were humanely killed, and the tumours were resected on day 40 after cell injection. One mouse tumour in Crizotinib group was completely eliminated. **e, f** After transplantation of cells into mice, the tumour volume of each mouse was measured continuously. **g** The volume of the resected tumours was determined. **h, i** Serial measures of mouse weight were taken after cells had been transplanted into mice. **j** The weight of the resected tumours was determined. **k** Western blotting analysis was performed to detect the phosphorylated and total protein levels of SMAD2 and Erk in resected tumours tissue (left). Right: the summary data of western blotting show the level of p-SMAD2 and p-Erk in Lewis. The data shown are means ± SD. ***$p < 0.001$; **$p < 0.01$; *$p < 0.05$; ns not significant $p > 0.05$. Scale bar, 200 μm.

Q. Liang et al.

DATA AVAILABILITY

All data generated or analysed during this study are included in this published article and its supplementary information files.

REFERENCES

1. Cooper CS, Park M, Blair DG, Tainsky MA, Huebner K, Croce CM, et al. Molecular cloning of a new transforming gene from a chemically transformed human cell line. Nature. 1984;311:29–33.
2. Drilon A, Cappuzzo F, Ou SI, Camidge DR. Targeting MET in lung cancer: will expectations finally be MET? J Thorac Oncol. 2017;12:15–26.
3. Gherardi E, Birchmeier W, Birchmeier C, Vande Woude G Targeting MET in cancer: rationale and progress. Nat Rev Cancer. 2012;12:89–103.
4. Peng S, Wang R, Zhang X, Ma Y, Zhong L, Li K, et al. EGFR-TKI resistance promotes immune escape in lung cancer via increased PD-L1 expression. Mol Cancer. 2019;18:165.
5. Hughes VS, Siemann DW. Have clinical trials properly assessed c-Met inhibitors? Trends Cancer. 2018;4:94–7.
6. Westover D, Zugazagoitia J, Cho BC, Lovly CM, Paz-Ares L. Mechanisms of acquired resistance to first- and second-generation EGFR tyrosine kinase inhibitors. Ann Oncol. 2018;29:i10–9.
7. Cortot AB, Kherrouche Z, Descarpentries C, Wislez M, Baldacci S, Furlan A, et al. Exon 14 deleted MET receptor as a new biomarker and target in cancers. J Natl Cancer Inst. 2017;109.
8. Lee CC, Yamada KM. Identification of a novel type of alternative splicing of a tyrosine kinase receptor. Juxtamembrane deletion of the c-met protein kinase C serine phosphorylation regulatory site. J Biol Chem. 1994;269:19457–61.
9. Lee JH, Gao CF, Lee CC, Kim MD, Vande Woude GF. An alternatively spliced form of Met receptor is tumorigenic. Exp Mol Med. 2006;38:565–73.
10. Lee JM, Kim B, Lee SB, Jeong Y, Oh YM, Song YJ, et al. Cbl-independent degradation of Met: ways to avoid agonism of bivalent Met-targeting antibody. Oncogene. 2014;33:34–43.
11. Socinski MA, Pennell NA, Davies KD. MET exon 14 skipping mutations in non-small-cell lung cancer: an overview of biology, clinical outcomes, and testing considerations. JCO Precis Oncol. 2021;5:PO.20.00516.
12. Frampton GM, Ali SM, Rosenzweig M, Chmielecki J, Lu X, Bauer TM, et al. Activation of MET via diverse exon 14 splicing alterations occurs in multiple tumor types and confers clinical sensitivity to MET inhibitors. Cancer Discov. 2015;5:850–9.
13. Ma PC, Kijima T, Maulik G, Fox EA, Sattler M, Griffin JD, et al. c-MET mutational analysis in small cell lung cancer: novel juxtamembrane domain mutations regulating cytoskeletal functions. Cancer Res. 2003;63:6272–81.
14. Heist RS, Sequist LV, Borger D, Gainor JF, Arellano RS, Le LP, et al. Acquired resistance to crizotinib in NSCLC with MET exon 14 skipping. J Thorac Oncol. 2016;11:1242–5.
15. Cancer Genome Atlas Research Network. Author Correction: Comprehensive molecular profiling of lung adenocarcinoma. Nature. 2018;559:E12.
16. Tong JH, Yeung SF, Chan AW, Chung LY, Chau SL, Lung RW, et al. MET amplification and exon 14 splice site mutation define unique molecular subgroups of non-small cell lung carcinoma with poor prognosis. Clin Cancer Res. 2016;22:3048–56.
17. Rotow JK, Gui P, Wu W, Raymond VM, Lanman RB, Kaye FJ, et al. Co-occurring alterations in the RAS-MAPK pathway limit response to MET inhibitor treatment in MET exon 14 skipping mutation-positive lung cancer. Clin Cancer Res. 2020;26:439–49.
18. Suzawa K, Offin M, Lu D, Kurzatkowski C, Vojnic M, Smith RS, et al. Activation of KRAS mediates resistance to targeted therapy in MET exon 14-mutant non-small cell lung cancer. Clin Cancer Res. 2019;25:1248–60.
19. Bahcall M, Awad MM, Sholl LM, Wilson FH, Xu M, Wang S, et al. Amplification of wild-type KRAS imparts resistance to crizotinib in MET exon 14 mutant non-small cell lung cancer. Clin Cancer Res. 2018;24:5963–76.
20. Drilon A, Clark JW, Weiss J, Ou SI, Camidge DR, Solomon BJ, et al. Antitumor activity of crizotinib in lung cancers harboring a MET exon 14 alteration. Nat Med. 2020;26:47–51.
21. Lu S, Fang J, Li X, Cao L, Zhou J, Guo Q, et al. Phase II study of savolitinib in patients (pts) with pulmonary sarcomatoid carcinoma (PSC) and other types of non-small cell lung cancer (NSCLC) harboring MET exon 14 skipping mutations (METex14+). J Clin Oncol. 2020;38:9519.
22. French R, Feng Y, Pauklin S. Targeting TGFbeta signalling in cancer: toward context-specific strategies. Trends Cancer. 2020;6:538–40.
23. Shi Y, Massague J. Mechanisms of TGF-beta signaling from cell membrane to the nucleus. Cell. 2003;113:685–700.
24. Loomans HA, Andl CD. Intertwining of activin A and TGFbeta signaling: dual roles in cancer progression and cancer cell invasion. Cancers (Basel). 2014;7:70–91.
25. Zhong G, Zhao Q, Chen Z, Yao T. TGF-beta signaling promotes cervical cancer metastasis via CDR1as. Mol Cancer. 2023;22:66.
26. Zhang J, van Dinther M, Thorikay M, Gourabi BM, Kruithof BPT, Ten Dijke P. Opposing USP19 splice variants in TGF-beta signaling and TGF-beta-induced epithelial-mesenchymal transition of breast cancer cells. Cell Mol Life Sci. 2023;80:43.
27. Vignjevic D, Montagnac G. Reorganisation of the dendritic actin network during cancer cell migration and invasion. Semin Cancer Biol. 2008;18:12–22.
28. Izdebska M, Zielinska W, Grzanka D, Gagat M. The role of actin dynamics and actin-binding proteins expression in epithelial-to-mesenchymal transition and its association with cancer progression and evaluation of possible therapeutic targets. Biomed Res Int. 2018;2018:4578373.
29. Mukai M, Sato S, Kimura T, Komatsu N, Ninomiya H, Nakasaki H, et al. Predicting the recurrence/metastasis of stage II and III breast cancer with lymph node metastasis. Oncol Rep. 2004;12:303–6.
30. Wang F, Liu Y, Qiu W, Shum E, Feng M, Zhao D, et al. Functional analysis of MET exon 14 skipping alteration in cancer invasion and metastatic dissemination. Cancer Res. 2022;82:1365–79.
31. Hao Y, Baker D, Ten Dijke P. TGF-beta-mediated epithelial-mesenchymal transition and cancer metastasis. Int J Mol Sci. 2019;20:2767.
32. Buwaneka P, Ralko A, Gorai S, Pham H, Cho W. Phosphoinositide-binding activity of Smad2 is essential for its function in TGF-beta signaling. J Biol Chem. 2021;297:101303.
33. Collie GW, Koh CM, O'Neill DJ, Stubbs CJ, Khurana P, Eddershaw A, et al. Structural and molecular insight into resistance mechanisms of first generation cMET inhibitors. ACS Med Chem Lett. 2019;10:1322–7.
34. Desai A, Cuellar S. The current landscape for METex14 skipping mutations in non-small cell lung cancer. J Adv Pract Oncol. 2022;13:539–44.
35. Peschard P, Park M. Escape from Cbl-mediated downregulation: a recurrent theme for oncogenic deregulation of receptor tyrosine kinases. Cancer Cell. 2003;3:519–23.
36. Hong L, Zhang J, Heymach J V, Le X. Current and future treatment options for MET exon 14 skipping alterations in non-small cell lung cancer. Ther Adv Med Oncol. 2021;13:1758835921992976.
37. Cortot A, Le X, Smit E, Viteri S, Kato T, Sakai H, et al. Safety of MET tyrosine kinase inhibitors in patients with MET exon 14 skipping non-small cell lung cancer: a clinical review. Clin Lung Cancer. 2022;23:195–207.
38. Wolf J, Garon EB, Groen HJM, Tan DSW, Gilloteau I, Le Mouhaer S, et al. Patient-reported outcomes in capmatinib-treated patients with METex14-mutated advanced NSCLC: results from the GEOMETRY mono-1 study. Eur J Cancer. 2022;183:98–108.
39. Babey H, Jamme P, Curcio H, Assie JB, Veillon R, Doubre H, et al. Real-world treatment outcomes of MET exon14 skipping in non-small cell lung cancer: GFPC 03-18 study. Target Oncol. 2023;18:585–91.
40. Yan SB, Um SL, Peek VL, Stephens JR, Zeng W, Konicek BW, et al. MET-targeting antibody (emibetuzumab) and kinase inhibitor (merestinib) as single agent or in combination in a cancer model bearing MET exon 14 skipping. Invest New Drugs. 2018;36:536–44.
41. Knowles LM, Stabile LP, Egloff AM, Rothstein ME, Thomas SM, Gubish CT, et al. HGF and c-Met participate in paracrine tumorigenic pathways in head and neck squamous cell cancer. Clin Cancer Res. 2009;15:3740–50.
42. Lengyel E, Prechtel D, Resau JH, Gauger K, Welk A, Lindemann K, et al. C-Met overexpression in node-positive breast cancer identifies patients with poor clinical outcome independent of Her2/neu. Int J Cancer. 2005;113:678–82.
43. Joffre C, Barrow R, Menard L, Calleja V, Hart IR, Kermorgant S. A direct role for Met endocytosis in tumorigenesis. Nat Cell Biol. 2011;13:827–37.
44. Li X, Wu Y, Tian T. TGF-beta signaling in metastatic colorectal cancer (mCRC): from underlying mechanism to potential applications in clinical development. Int J Mol Sci. 2022;23:14436.
45. Wang Y, Shi J, Chai K, Ying X, Zhou BP. The role of snail in EMT and tumorigenesis. Curr Cancer Drug Targets. 2013;13:963–72.
46. Bakiri L, Macho-Maschler S, Custic I, Niemiec J, Guio-Carrion A, Hasenfuss SC, et al. Fra-1/AP-1 induces EMT in mammary epithelial cells by modulating Zeb1/2 and TGFbeta expression. Cell Death Differ. 2015;22:336–50.
47. Zhou H, Li L, Xie W, Wu L, Lin Y, He X. TAGLN and High-mobility Group AT-Hook 2 (HMGA2) complex regulates TGF-beta-induced colorectal cancer metastasis. Onco Targets Ther. 2020;13:10489–98.
48. Zhu S, Wang W, Clarke DC, Liu X. Activation of Mps1 promotes transforming growth factor-beta-independent Smad signaling. J Biol Chem. 2007;282:18327–38.
49. Pilotto S, Gkountakos A, Carbognin L, Scarpa A, Tortora G, Bria E. MET exon 14 juxtamembrane splicing mutations: clinical and therapeutical perspectives for cancer therapy. Ann Transl Med. 2017;5:2.
50. Salgia R, Sattler M, Scheele J, Stroh C, Felip E. The promise of selective MET inhibitors in non-small cell lung cancer with MET exon 14 skipping. Cancer Treat Rev. 2020;87:102022.
51. Kang J, Deng QM, Feng W, Chen ZH, Su JW, Chen HJ, et al. Response and acquired resistance to MET inhibitors in de novo MET fusion-positive advanced non-small cell lung cancer. Lung Cancer. 2023;178:66–74.

AUTHOR CONTRIBUTIONS

FUNDING

COMPETING INTERESTS

The authors declare no competing interests.

ETHICS APPROVAL AND CONSENT TO PARTICIPATE

All procedures performed in studies involving animals were in accordance with the ethical standards of the Department of Laboratory Animal Science of Fudan University.

CONSENT FOR PUBLICATION

All authors read and approved the final manuscript.

ADDITIONAL INFORMATION

Supplementary information The online version contains supplementary material available at https://doi.org/10.1038/s41416-023-02495-5.

Correspondence and requests for materials should be addressed to Min Yu, Huijie Wang or Bing Zhao.

Reprints and permission information is available at http://www.nature.com/reprints

Publisher's note Springer Nature remains neutral with regard to jurisdictional claims in published maps and institutional affiliations.